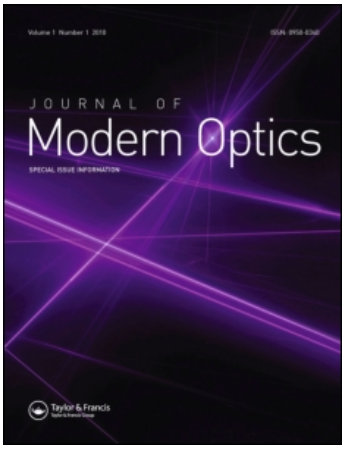

Journal of Modern Optics
Publication details, including instructions for authors and subscription information:
http://www.informaworld.com/smpp/title~content=t713191304

Polarisation states of high harmonic generation from aligned molecules

Anh-Thu Le[a]; C. D. Lin[a]
[a] Department of Physics, Cardwell Hall, Kansas State University, Manhattan, KS 66506, USA

First published on: 07 March 2011

To cite this Article Le, Anh-Thu and Lin, C. D.(2011) 'Polarisation states of high harmonic generation from aligned molecules', Journal of Modern Optics,, First published on: 07 March 2011 (iFirst)
To link to this Article: DOI: 10.1080/09500340.2011.564737
URL: http://dx.doi.org/10.1080/09500340.2011.564737

Journal of Modern Optics
2011, 1–8, iFirst

Polarisation states of high harmonic generation from aligned molecules

Anh-Thu Le* and C.D. Lin

Department of Physics, Cardwell Hall, Kansas State University, Manhattan, KS 66506, USA

(*Received 26 January 2011; final version received 15 February 2011*)

We present detailed theoretical calculations based on the recently developed quantitative rescattering theory (QRS) for polarisation and ellipticity of high-order harmonics from aligned N_2 and O_2 generated with mid-infrared linearly polarised laser pulses. Within the QRS, the two polarisation states of high-order harmonics are due to the high-energy photons emitted with polarisation parallel or perpendicular to the direction of the same returning electron wave packet in the photo-recombination process. The complex transition dipoles responsible for these two components have, in general, difference phases, which results in the ellipticity of emitted harmonics. Our results show clear target-species dependent polarisation states. In particular, we found strong harmonic ellipticity in aligned N_2, but weak ellipticity in aligned O_2 for harmonics below 100 eV. We further show the factorisation of the macroscopic high harmonic generation under typical experimental conditions. This implies that results of polarisation measurements are quite robust to the macroscopic phase matching conditions.

Keywords: high-harmonic generation; intense lasers; molecular alignment

1. Introduction

High-order harmonic generation (HHG), one of the most important nonlinear processes, occurs when an atomic or molecular gas is placed in an intense laser field [1]. Due to the symmetry, the emitted HHG is polarised parallel to the driving laser polarisation if the gas is isotropic, as in case of atomic or unaligned molecular targets. However, for aligned molecules, a harmonic component perpendicular to the driving laser polarisation is expected to be present [2]. Clearly, one needs a good level of molecular alignment in order to produce a sufficient amount of HHG perpendicular component as it goes to zero for the isotropic case. It is therefore not surprising that polarisation measurements for emitted harmonics were reported only quite recently [3–6]. These experimental data on harmonic polarisation from aligned N_2, O_2, and CO_2 showed target-species dependent features which give complementary information on the molecular structure of the targets. The polarisation-resolved measurement technique has also been used in order to enhance the signal-to-background ratio in HHG experiments [5]. All these experiments were carried out within the pump-probe scheme, where a relatively weak, short laser pulse (the pump) is used to impulsively align the molecules along the pump laser polarisation direction, and after some delay time, a second laser pulse (the probe) is used to generate high-order harmonics.

It is well known that information about the target is contained in the HHG signals. To fully characterise the target, both components of HHG are needed. For example, in the tomographic procedure of extracting the highest occupied molecular orbital (HOMO), intensities for both HHG polarisation states together with their phases are needed in principle [7,8]. It has been noted already in [3] that the theoretical simulation based on the strong-field approximation (SFA) cannot quantitatively reproduce the polarisation experimental measurements. In fact, the SFA does not predict the ellipticity of the emitted harmonic, at least in the standard stationary-phase approximation [9]. It is therefore somewhat a surprise when Zhou and co-workers [10] reported a strong ellipticity in harmonic emission from strongly aligned N_2. Clearly, these important findings present a challenge for the accurate theoretical description of HHG.

Theoretical calculations of polarisation and ellipticity of HHG from aligned molecules have been reported recently [9,11–14]. These calculations were based on different theoretical models and their predictions differ somewhat from one another. Furthermore, these earlier calculations compared a single-molecule response directly with experimental data, without accounting for the macroscopic propagation. Clearly, further investigation is needed in order to resolve the discrepancy among the theories as well as between theory and experiment.

*Corresponding author. Email: atle@phys.ksu.edu

ISSN 0950–0340 print/ISSN 1362–3044 online

DOI: 10.1080/09500340.2011.564737
http://www.informaworld.com

As mid-infrared (mid-IR) intense laser pulses are becoming available [15–17], in the future it could be possible to extend HHG polarisation measurements to much higher photon energies. In this paper, we extend our recent calculations [13] for polarisation and ellipticity of HHG from aligned N_2 and O_2 to energies up to 150 eV with mid-IR laser of 2000 nm wavelength. At the single-molecule level, our calculations are based on the recently developed quantitative rescattering theory (QRS) [18–22]. We show that target-species dependent features become even more pronounced with a mid-IR laser. We also show semi-analytically the factorisation of the macroscopic HHG and further discuss the effect of macroscopic propagation on the polarisation states of HHG.

2. Theoretical method

In the QRS, each of the two components of the complex induced dipole, is represented as a product of a returning electron wave packet and the laser-free photo-recombination transition dipole,

$$D_{\parallel,\perp}(\omega,\vartheta) = W(E_k,\vartheta)\, d_{\parallel,\perp}(\omega,\vartheta). \tag{1}$$

Here ϑ is the angle between the molecular axis and the (probe) laser polarisation direction E_k is the 'incident' energy of the returning electron, and $\omega = I_p + E_k$ is the emitted photon energy, with I_p being the ionisation potential. Note that the wave packet $W(E_k,\vartheta)$ is the same for both components. The returning electron can recombine with the parent ion to emit a photon with polarisation in the parallel or perpendicular direction to its motion, resulting in the two polarisation components of the emitted harmonics observed in the experiment. The (complex) transition dipoles $d_{\parallel,\perp}$ are obtained in our calculations from state-of-the-art molecular photoionisation code [23,24] for each fixed-in-space molecule. Note that we only need to consider the harmonic components on the plane perpendicular to the propagation direction of the driving laser, since only the harmonic emission propagating along this direction can be efficiently phase matched. As for the returning electron wave packet, we extract it from the SFA [19]. We comment that the wave packet can also be extracted by solving the time-dependent Schrödinger equation (TDSE) for a reference atom [19].

For comparison with experiments, induced dipoles $D_\parallel(\omega,\vartheta)$ and $D_\perp(\omega,\vartheta)$ from fixed-in-space molecules are coherently convoluted with the molecular alignment distribution [2,19]. Assume that the pump and probe laser pulses propagate collinearly and α is the angle between the two polarisation directions. Let $\theta(\vartheta)$ and $\phi(\varphi)$ be the polar and azimuthal angles of the molecular axis in the frame attached to the pump (probe) field. These angles are related by

$$\cos\theta = \cos\vartheta\cos\alpha + \sin\vartheta\sin\alpha\cos\varphi. \tag{2}$$

We carry out alignment averaging in the 'probe frame, in which the alignment distribution is

$$\rho(\alpha,\vartheta,\phi) = \rho(\theta(\alpha,\vartheta,\varphi)). \tag{3}$$

Here we have used the fact that the alignment distribution in the 'pump' frame does not depend on azimuthal angle ϕ. Furthermore, for linear molecules, we have

$$D_\parallel(\omega,\vartheta,\varphi) = D_\parallel(\omega,\vartheta), \tag{4}$$

and

$$D_\perp(\omega,\vartheta,\varphi) = D_\perp(\omega,\vartheta,\varphi=0)\cos\varphi. \tag{5}$$

Therefore, the alignment averaged induced dipoles can be written as

$$\overline{D}_\parallel(\omega,\alpha) = \int_0^\pi\int_0^{2\pi} D_\parallel(\omega,\vartheta)\rho(\alpha,\vartheta,\varphi)\sin\vartheta\,\mathrm{d}\vartheta\,\mathrm{d}\varphi. \tag{6}$$

for the parallel component, and

$$\begin{aligned}\overline{D}_\perp(\omega,\alpha) &= \int_0^\pi\int_0^{2\pi} D_\perp(\omega,\vartheta,\varphi)\rho(\alpha,\vartheta,\varphi)\sin\vartheta\,\mathrm{d}\vartheta\,\mathrm{d}\varphi \\ &= \int_0^\pi\int_0^{2\pi} D_\perp(\omega,\vartheta,\varphi=0)\rho(\alpha,\vartheta,\varphi) \\ &\quad\times\cos\varphi\sin\vartheta\,\mathrm{d}\vartheta\,\mathrm{d}\varphi,\end{aligned} \tag{7}$$

for the perpendicular component. These equations show explicitly that we only need to calculate transition dipoles $d_{\parallel,\perp}(\omega,\vartheta)$ for $\varphi = 0$. By comparing Equation (6) with Equation (7) it follows that the averaging tends to favor the parallel component. It is also clear from Equation (7) that for isotropic distribution ($\rho = 1$) or for the case of parallel pump-probe polarisations (ρ is independent of φ) the integration over φ in Equation (7) goes to zero. In other words, there exists only parallel component of HHG in those cases. (This result is obvious due to symmetry argument since the probe polarisation defines the only direction in those systems.) To get intensities and phases for harmonic fields of both components from a macroscopic medium, the averaged induced dipoles need to be fed into the macroscopic propagation equation. We will discuss this issue in Section 4.

3. Polarisation states of HHG: a single-molecule picture

In our simulations, the alignment distribution ρ is obtained from numerical solution of the TDSE within

the rotor model for each molecular species [19,25]. We use a 120 fs pump laser pulse of 800 nm wavelength with an intensity of $3 \times 10^{13}\,\mathrm{W/cm^2}$. The rotational temperature is assumed to be 100 K. These parameters were chosen to closely match the typical experimental conditions [10]. We vary angles between pump and probe polarisations α and keep the time delay at half revival for N_2 and O_2. We use a 30 fs driving laser pulse of 2000 nm wavelength (photon energy of 0.62 eV) with an intensity of $1.25 \times 10^{14}\,\mathrm{W/cm^2}$. For N_2 and O_2, the HHG cutoff is near harmonic order 260 (H260), or photon energy near 160 eV.

First, we show in Figure 1(*a*) and 1(*b*) the theoretical intensity ratio $\frac{I_\perp}{I_\parallel}$ between perpendicular and parallel components for a few harmonic orders from H49 to H249 from N_2 and O_2, respectively, as a function of angle α between pump and probe polarisations. The intensity ratio is about one order of magnitude smaller in O_2, than in N_2, except for very high harmonics near H249. For N_2, the intensity ratio reaches 0.15 at the peak near 55° for H49. It then slowly decreases as harmonic order increases. In the meanwhile, its peak first shifts to smaller pump-probe angles below H99 and then shifts to larger pump-probe angles above H99. This behaviour is totally different from the O_2 case. For O_2, the intensity ratio reaches only 0.01 at its peak near 35° for H49. It then decreases with increased harmonic order below H149, but it increases for harmonics above H149. Its peak shifts to pump-probe angle α near 20° at H249. As we will see below, these differences in N_2 and O_2 are direct consequences of their photo-recombination (or the photoionisation) cross-sections. We comment that for both targets, the intensity ratio goes to zero if pump and probe polarisations are parallel ($\alpha = 0$) or perpendicular ($\alpha = 90°$), as one can expect from symmetry consideration.

Since the same wave packet is responsible for both HHG components, it is clear from Equation (1) that in order to understand the origin of the polarisation states of HHG, we need to compare the two components of transition dipoles $d_\parallel$ and $d_\perp$. We show in Figure 2 photoionisation differential cross-sections for N_2 and O_2, corresponding to the parallel and perpendicular components of emitted harmonics H99, H149, H199, and H249. These cross-sections are proportional to $|d_\parallel|^2$ and $|d_\perp|^2$, respectively. Together with the phases (not shown), these data are used for obtaining induced dipoles $D_\parallel(\omega, \vartheta)$ and $D_\perp(\omega, \vartheta)$ in our calculations by using Equation (1).

Overall, the perpendicular components $|d_\perp|$ are relatively smaller than the parallel components $|d_\parallel|$ for both targets. First we discuss low harmonic orders near H99 and below. Experimentally, this energy range is already accessible by using lasers of 800 nm wavelength [3,10]. In this energy range, $|d_\perp|$ are quite comparable with $|d_\parallel|$ for N_2, but not so for O_2. Equation (1) of the QRS would predict large (small) intensity ratio between perpendicular and parallel components of HHG for N_2 (O_2). This is consistent with the results shown in Figure 1. In fact, this behaviour has been found experimentally [3,10] and theoretically explained [13] in the case of an 800 nm probe laser.

As harmonic order increases, $|d_\parallel|$ for both N_2 and O_2 decrease and their alignment dependence is nearly unchanged for harmonics above H149. For O_2, a shallow minimum near 45° can be seen in the cross-section for harmonic orders above H199. This minimum is related to the 'interference minimum' in HHG spectra from aligned O_2 at high photon energies, as has been noted in [19]. As for $|d_\perp|$, it decreases with increased harmonic order for N_2 but stays almost unchanged for O_2. These facts explain why the

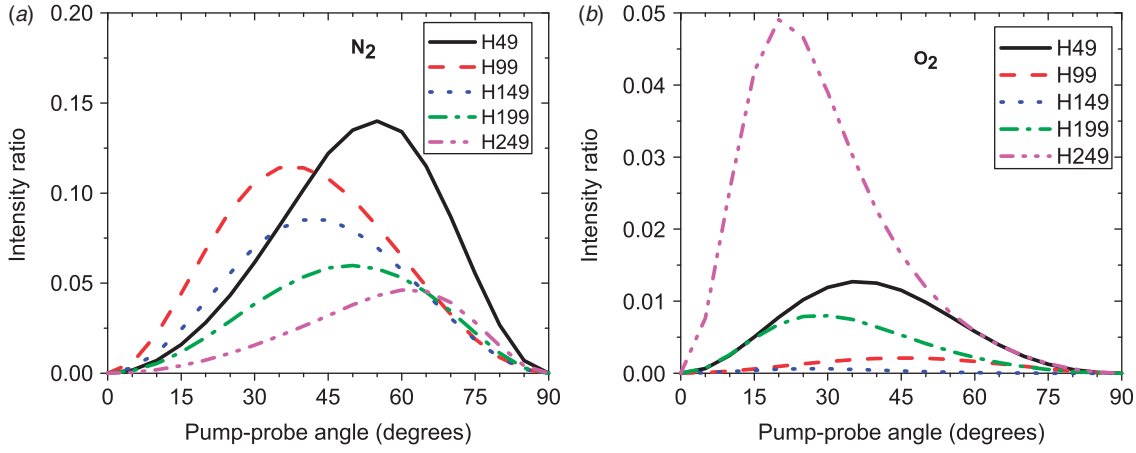

Figure 1. Intensity ratios between perpendicular and parallel component of the HHG fields, as a function of alignment angle between pump and probe polarisation directions, for N_2 (*a*) and O_2 (*b*). (The colour version of this figure is included in the online version of the journal.)

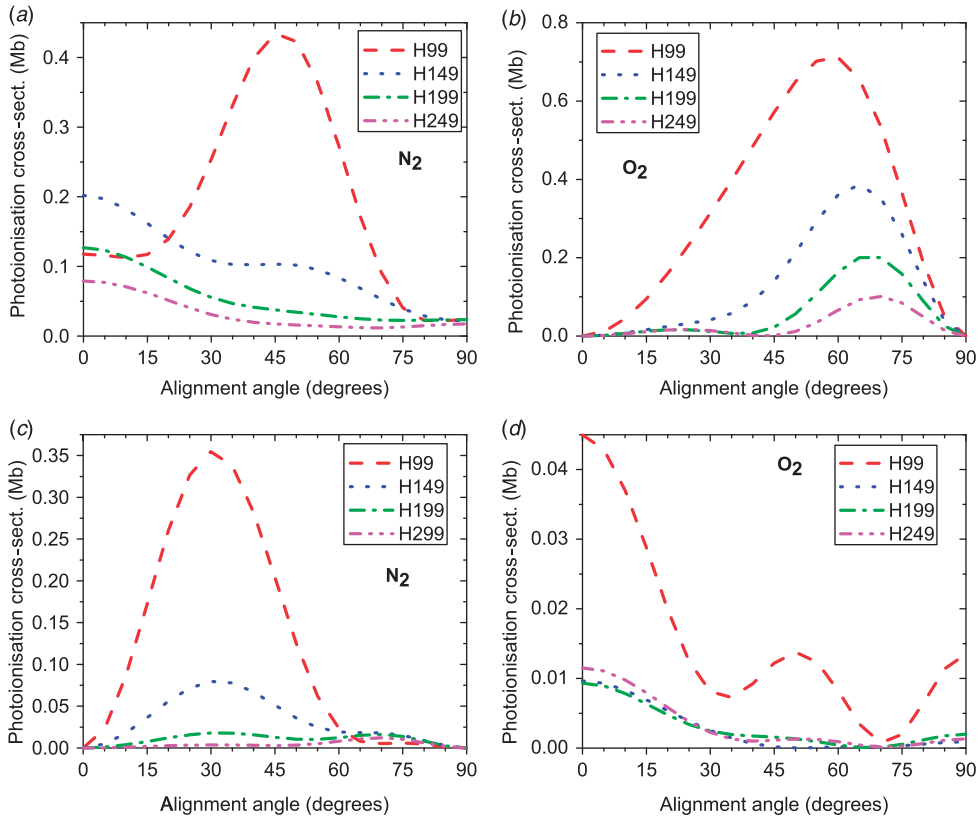

Figure 2. Photoionisation differential cross-sections, corresponding to the parallel component of emitted harmonics versus alignment angle between molecular axis and polarisation direction. Cross-sections are shown for energies corresponding to H99, H149, H199, and H249 for N_2 (*a*) and O_2 (*b*). Cross-sections, corresponding to the perpendicular component of HHG are shown in (*c*) and (*d*), for N_2 and O_2, respectively. (The colour version of this figure is included in the online version of the journal.)

intensity ratio decreases for N_2, but increase for O_2 at high harmonic orders above H149, as seen in Figure 1.

From the intensity ratio one can calculate the orientation angle ϕ of the emitted harmonic polarisation (defined with respect to the direction of the probe laser polarisation) as

$$\tan(\phi) = \tan(\gamma) \equiv \sqrt{\frac{I_\perp}{I_\parallel}}. \tag{8}$$

This has been used by Levesque and colleagues [3]. However, if the phase difference δ between perpendicular and parallel components of harmonic field is different from 0 (or π), the emitted harmonic becomes elliptically polarised, with the orientation angle of the ellipse defined as [26]

$$\tan(2\phi) = \tan(2\gamma)\cos(\delta). \tag{9}$$

In our calculations we use the latter formula, as the phase difference δ obtained from the QRS is, in general, different from 0 (or π).

Our results for the orientation angle ϕ are shown as color-coded plots in Figure 3(*a*) and (*b*) for N_2 and O_2, respectively, as a function of alignment angle α between pump and probe polarisations and harmonic order. Here we use the same convention as in Zhou and colleagues [10], where ϕ and α are positive (negative) for clockwise (counterclockwise) rotation from the direction of the electric field of the probe laser. The results are antisymmetric with respect to the sign change in the pump-probe angle α. Overall, the HHG ellipse orientation images are very different for the two targets, which reflects differences in their photoionisation cross-sections and dipole phases. We note that the energy range below H99 can be explored by using 800 nm lasers. In fact, in this low energy range, the present results from 2000 nm lasers are very close to our previous results with 800 nm lasers [13], which reproduced very well the experimental measurements [3,10]. In particular, we see a sign change in the orientation angle as a function of harmonic order near H47 for N_2. This corresponds to the harmonic photon energy of 30 eV, the same energy, where the sign changes if an 800 nm laser is used [13]. This sign change is nearly independent of the pump-probe polarisation angle. The orientation angle is also much smaller in O_2,

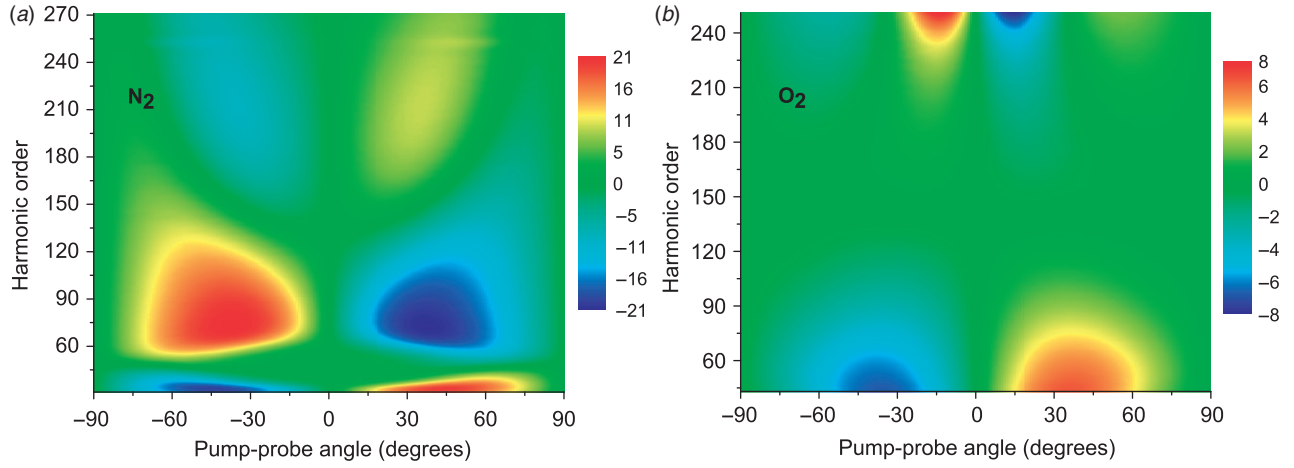

Figure 3. Colour-coded plot of the orientation angle (in degrees) as a function of alignment angle α between pump and probe polarisation directions and harmonic order for N_2 (*a*) and O_2 (*b*). (The colour version of this figure is included in the online version of the journal.)

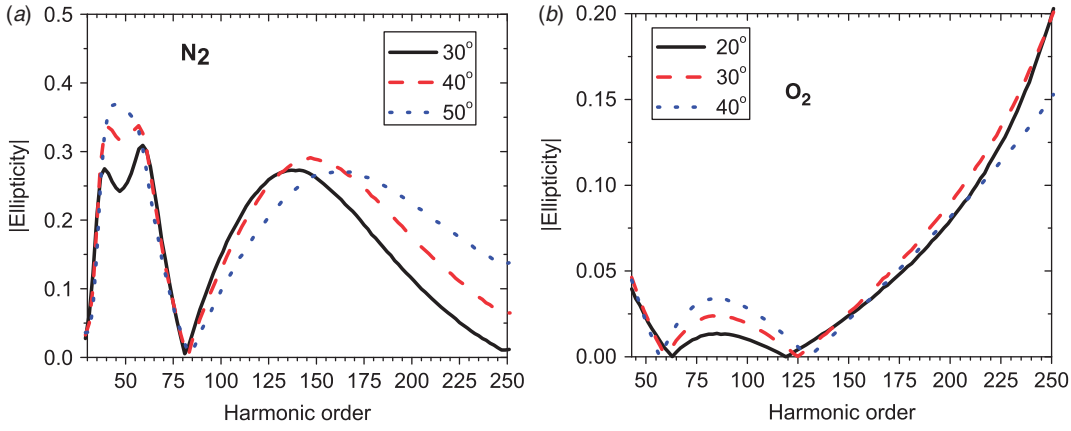

Figure 4. Absolute value of harmonic ellipticity as a function of harmonic orders at different alignment angles α shown in the labels for N_2 (*a*) and O_2 (*b*). (The colour version of this figure is included in the online version of the journal.)

reaching about 7° as compared to about 20° in N_2. We further note that the increased orientation angles near $\alpha = \pm 20°$ in O_2 is related to the 'interference minimum' in the photoionisation cross-sections corresponding to the parallel HHG components.

For completeness we show in Figure 4 the absolute value of ellipticity ϵ of emitted harmonics from N_2 and O_2. These data can be used to compare directly with future experiments. Ellipticity can be calculated by using

$$\epsilon = \tan(\chi), \tag{10}$$

with χ defined as [28]

$$\sin(2\chi) = \sin(2\gamma)\sin(\delta). \tag{11}$$

Overall, our calculations show quite large ellipticity for N_2 and very small ellipticity for O_2 under the same condition for both pump and probe lasers. For N_2, the ellipticity reaches almost ≈0.4, and it is about an order of magnitude larger than that of O_2 below H149. But the harmonic ellipticity from O_2 increases significantly for harmonics above H199.

4. Effect of macroscopic propagation

So far we have presented our calculations within a single-molecule picture. In order to really compare with experiment, macroscopic propagation of the driving field and harmonic fields needs to be carried out [27,28]. However, under typical experimental conditions, it is possible to show that the macroscopic propagation will affect both harmonic components in the same way. Indeed, the propagation equation for each harmonic component E_a (with $a = \parallel$ or $\perp$) in an

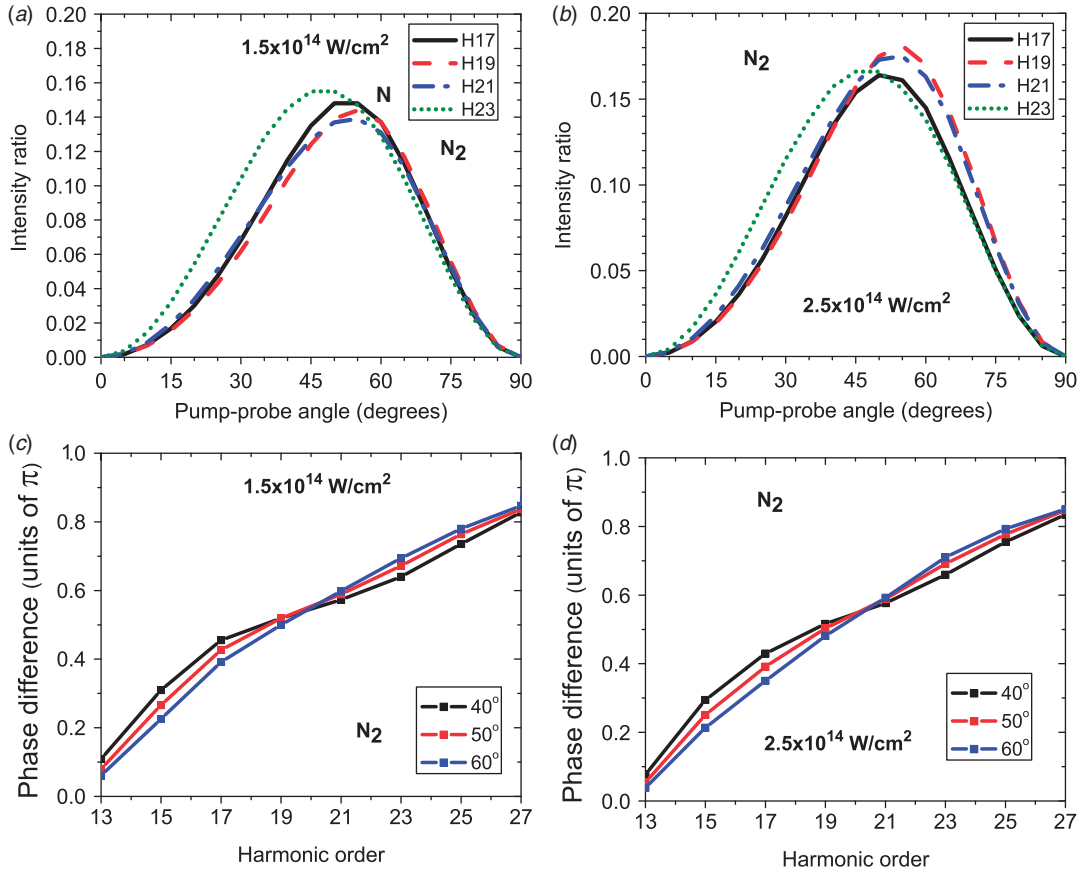

Figure 5. Intensity ratio between perpendicular and parallel component of the HHG fields for few selected harmonics as a function of the angle between pump and probe polarisations at laser intensities of 1.5×10^{14} W/cm^2 (*a*) and 2.5×10^{14} (*b*). The phase difference between the two polarisation components are shown in (*c*) and (*d*) for few alignment angles near the peak of the intensity ratio. The driving laser is of 800 nm wavelength. (The colour version of this figure is included in the online version of the journal.)

aligned molecular gas medium can be written under the paraxial approximation as [27,28]

$$\nabla_{\perp}^2 E_a(r,z,\omega,\alpha) - \frac{2i\omega}{c}\frac{\partial E_a(r,z,\omega,\alpha)}{\partial z} \propto \overline{D}_a(r,z,\omega,\alpha), \tag{12}$$

where $\overline{D}_{\parallel,\perp}(r,z,\omega,\alpha)$ is the nonlinear polarisation at the position $\{r,z\}$ in the gas jet, averaged over the molecular alignment distribution for a fixed pump-probe angle α (see Equations (6) and (7)). Here we assume that absorption and dispersion are negligible. In a typical gas jet experiment, the aligning laser is much less intense and more loosely focused than the probe laser. Therefore, in the interaction volume of the probe laser within the gas jet, the aligning laser can be assumed to be uniform.

To be specific, we will discuss below the case of N_2. For illustration purposes we use an 800 nm laser as the probe. We found that for a fixed $\{\omega,\alpha\}$ the intensity ratio and phase difference between the two components $\overline{D}_{\parallel}(\omega,\alpha)$ and $\overline{D}_{\perp}(\omega,\alpha)$ change only about 10% as the probe laser intensity changes from 1.5×10^{14} to 2.5×10^{14} W/cm^2. This comparison is shown in Figure 5 (see also Figure 2(*a*) for a laser intensity of 2×10^{14} W/cm^2). This means that the ratio $R = |\overline{D}_{\perp}/\overline{D}_{\parallel}|$ and phase difference are nearly independent on the spatial coordinates $\{r,z\}$ within the interaction volume. From Equation (12), it follows that ratio $|E_{\perp}/E_{\parallel}| = R$. The same arguments also hold for the phase difference. This implies that the results presented in the previous section should be nearly unchanged even if the macroscopic propagation is carried out. Our results still depend on the degree of molecular alignment, which is controlled by the pump pulse. Therefore, polarisation resolved measurements for HHG allow us to directly extract a single-molecule feature (up to averaging over the alignment distribution) without much influence of the details of the macroscopic phase-matching conditions.

This result is not entirely surprising. In fact, this can be seen more easily if we use the QRS formulation with the help of a reference atom [19]. More

specifically, the shape of the returning electron wave packet has been shown to be largely independent of the target. It can be written as (up to a constant phase and a constant factor due to ionisation rate of a reference atom) [19]

$$W(E_k, \vartheta) \propto \sqrt{N(\vartheta)} W^{ref}(E_k), \tag{13}$$

where $N(\vartheta)$ is the ionisation probability for the emission along the laser polarisation direction, which depends on the molecular alignment angle ϑ, and $W^{ref}(E_k)$ is the returning wave packet for a reference atom. $N(\vartheta)$ can be calculated by using the SFA. It can also be approximated by using the molecular tunneling ionisation rate (MO-ADK) [29]. Note that in the tunneling regime the shape of $N(\vartheta)$ depends very weakly on laser intensity. By using Equations (1) and (13), Equations (6) and (7) can be expressed as

$$\overline{D}_{\parallel,\perp}(\omega, \alpha) \propto W^{ref}(\omega) \overline{d}_{\parallel,\perp}(\omega, \alpha), \tag{14}$$

where the 'averaged' transition dipoles, weighted with the ionisation rate, are defined as

$$\overline{d}_{\parallel}(\omega, \alpha) = \int_0^{\pi} \int_0^{2\pi} \sqrt{N(\vartheta)} d_{\parallel}(\omega, \vartheta) \rho(\alpha, \vartheta, \varphi) \sin \vartheta \, \mathrm{d}\vartheta \, \mathrm{d}\varphi, \tag{15}$$

and

$$\overline{d}_{\perp}(\omega, \alpha) = \int_0^{\pi} \int_0^{2\pi} \sqrt{N(\vartheta)} d_{\perp}(\omega, \vartheta) \rho(\alpha, \vartheta, \varphi) \times \cos \varphi \sin \vartheta \, \mathrm{d}\vartheta \, \mathrm{d}\varphi. \tag{16}$$

From Equation (14) it follows that

$$\overline{D}_{\perp}(\omega, \alpha) / \overline{D}_{\parallel}(\omega, \alpha) = \overline{d}_{\perp}(\omega, \alpha) / \overline{d}_{\parallel}(\omega, \alpha). \tag{17}$$

In other words, for a fixed $\{\omega, \theta\}$ the ratio $\overline{D}_{\perp} / \overline{D}_{\parallel}$ does not depend on the probe laser parameters, and is totally determined by the ratio of the averaged transition dipoles. This is consistent with the results shown in Figure 5.

Inserting Equation (14) in Equation (12) gives

$$\nabla_{\perp}^2 E_a(r, z, \omega, \alpha) - \frac{2i\omega}{c} \frac{\partial E_a(r, z, \omega, \alpha)}{\partial z} \propto W^{ref}(r, z, \omega) \overline{d}_a(\omega, \alpha), \tag{18}$$

where $a = \parallel$ or $\perp$. Here we have written explicitly the dependence of the wave packet on the spatial coordinates $\{r, z\}$. Now let

$$E_a(r, z, \omega) = \overline{W}(r, z, \omega) \overline{d}_a(\omega, \alpha), \tag{19}$$

Equation (18) can then be rewritten as

$$\nabla_{\perp}^2 \overline{W}(r, z, \omega) - \frac{2i\omega}{c} \frac{\partial \overline{W}(r, z, \omega)}{\partial z} \propto W^{ref}(r, z, \omega). \tag{20}$$

The physical meaning of Equations (19) and (20) is quite clear. It implies that the simple factorisation in Equation (1) can be extended to a macroscopic medium, in which macroscopic HHG is a product of a macroscopic wave packet $\overline{W}(r, z, \omega)$ and an 'averaged' transition dipole. In fact, this is consistent with Jin and co-workers [28], who found this separation by numerically solving the propagation equation. This result is important for practical purposes if we wish to extract laser-independent target structure information from experiment. We comment that absorption and dispersion of high harmonics, which in principle are anisotropic for aligned molecules, cannot be neglected at high gas pressures. This leads to additional terms in Equation (12) and our arguments above are not applicable.

5. Conclusions

In conclusion, we have calculated polarisation and ellipticity of high-order harmonics from aligned N_2 and O_2 molecules generated with intense mid-infrared laser pulses. The use of long wavelength lasers allows us to explore harmonics with higher photon energies, which reveals stronger target-species dependent features of the polarisation states for N_2 and O_2, as compared with the case of near infrared lasers. We have analysed the macroscopic propagation effect and, in particular, we have identified experimental conditions under which the polarisation states are robust with respect to the macroscopic phase matching. We show that the use of the QRS drastically simplifies analysis of the macroscopic propagation of harmonics in the medium. Harmonic polarisation and ellipticity give valuable information about the target, and therefore are of critical importance for dynamic chemical imaging research. Our results clearly show that current theories are now capable of quantitatively explaining HHG experiments.

Acknowledgements

This work was supported in part by the Chemical Sciences, Geosciences and Biosciences Division, Office of Basic Energy Sciences, Office of Science, US Department of Energy.

References

[1] Brabec, T.; Krausz, F. *Rev. Mod. Phys.* **2000,** *72,* 545–591.
[2] Lein, M.; De Nalda, R.; Heesel, E.; Hay, N.; Springate, E.; Velotta, R.; Castillejo, M.; Knight, P.L.; Marangos, J.P. *J. Mod. Opt.* **2005,** *52,* 465–478.
[3] Levesque, J.; Mairesse, Y.; Dudovich, N.; Pepin, H.; Kieffer, J.C.; Corkum, P.B.; Villeneuve, D.M. *Phys. Rev. Lett.* **2007,** *98,* 183903.

[4] Mairesse, Y.; Levesque, J.; Dudovich, N.; Corkum, P.B.; Villeneuve, D.M. *J. Mod. Opt.* **2008,** *55,* 2591–2602.
[5] Mairesse, Y.; Dudovich, N.; Levesque, J.; Ivanov, M.Yu.; Corkum, P.B.; Villeneuve, D.M. *New J. Phys.* **2008,** *10,* 025028.
[6] Lee, G.H.; Kim, I.J.; Park, S.B.; Kim, T.K.; Nam, C.H. *Opt. Lett.* **2008,** *33,* 2083–2085.
[7] Itatani, J.; Levesque, J.; Zeidler, D; Pepin, H.; Kieffer, J.C.; Corkum, P.B.; Villeneuve, D.M. *Nature* **2004,** *432,* 867–871.
[8] Le, V.H.; Le, A.T.; Xie, R.H.; Lin, C.D. *Phys. Rev. A* **2007,** *76,* 013414.
[9] Etches, A.; Madsen, C.B.; Madsen, L.B. *Phys. Rev. A* **2010,** *81,* 013409.
[10] Zhou, X.; Lock, R.; Wagner, N.; Li, W.; Kapteyn, H.C.; Murnane, M.M. *Phys. Rev. Lett.* **2009,** *102,* 073902.
[11] Ramakrishna, S.; Sherratt, P.A.J.; Dutoi, A.D.; Seideman, T. *Phys. Rev. A* **2010,** *81,* 021802(R).
[12] Mairesse, Y.; Higuet, J.; Dudovich, N.; Shafir, D.; Fabre, B.; Mevel, E.; Constant, E.; Patchkovskii, S.; Walters, Z.; Ivanov, M.Yu.; Smirnova, O. *Phys. Rev. Lett.* **2010,** *104,* 213601.
[13] Le, A.T.; Lucchese, R.R.; Lin, C.D. *Phys. Rev. A* **2010,** *82,* 023814.
[14] Son, S.K.; Telnov, D.A.; Chu, S.I. *Phys. Rev. A* **2010,** *82,* 043829.
[15] Blaga, C.I.; Catoire, F.; Colosimo, P.; Paulus, G.G.; Muller, H.G.; Agostini, P.; DiMauro, L.F. *Nature Phys.* **2009,** *5,* 335–338.
[16] Torres, R.; Siegel, T.; Brugnera, L.; Procino, I.; Underwood, J.G.; Altucci, C.; Velotta, R.; Springate, E.; Froud, C.; Turcu, I.C.E.; Patchkovskii, S.; Ivanov, M.Yu.; Smirnova, O.; Marangos, J.P. *Phys. Rev. A* **2010,** *81,* 051802(R).
[17] Shiner, A.D.; Schmidt, B.E.; Trallero-Herrero, C.; Woerner, H.J.; Patchkovskii, S.; Corkum, P.B.; Kieffer, J.-C.; Legare, F.; Villeneuve, D.M. Probing Collective Multi-electron Dynamics with High Harmonic Spectroscopy – The Giant Resonance in Xenon. Nat. Phys., submitted for publication.
[18] Morishita, T.; Le, A.T.; Chen, Z.; Lin, C.D. *Phys. Rev. Lett.* **2008,** *100,* 013903.
[19] Le, A.T.; Lucchese, R.R.; Tonzani, S.; Morishita, T.; Lin, C.D. *Phys. Rev. A* **2009,** *80,* 013401.
[20] Le, A.T.; Morishita, T.; Lin, C.D. *Phys. Rev. A* **2008,** *78,* 023814.
[21] Le, A.T.; Picca, R.D.; Fainstein, P.D.; Telnov, D.A.; Lein, M.; Lin, C.D. *J. Phys. B* **2008,** *41,* 081002.
[22] Le, A.T.; Lucchese, R.R.; Lee, M.T.; Lin, C.D. *Phys. Rev. Lett.* **2009,** *102,* 203001.
[23] Stratmann, R.E.; Lucchese, R.R. *J. Chem. Phys.* **1995,** *102,* 8493–8505.
[24] Lucchese, R.R.; Raseev, G.; McKoy, V. *Phys. Rev. A* **1982,** *25,* 2572–2587.
[25] Stapelfeldt, H; Seideman, T. *Rev. Mod. Phys.* **2003,** *75,* 543–557.
[26] Born, M.; Wolf, E. *Principle of Optics*; Cambridge University Press: Cambridge, 1999.
[27] Gaarde, M.B.; Tate, J.L.; Schafer, K.J. *J. Phys. B* **2008,** *41,* 132001.
[28] Jin, C.; Le, A.T.; Lin, C.D. *Phys. Rev. A* **2009,** *79,* 053413.
[29] Tong, X.M; Zhao, Z.X.; Lin, C.D. *Phys. Rev. A* **2002,** *66,* 033402.